A Scale Analysis of Deep Moist Convection and Some Related Numerical Calculations

FRANK B. LIPPS AND RICHARD S. HEMLER

Geophysical Fluid Dynamics Laboratory/NOAA, Princeton University, Princeton, NJ 08540

(Manuscript received 6 December 1981, in final form 27 May 1982)

ABSTRACT

A scale analysis valid for deep moist convection is carried out. The approximate equations of motion are anelastic with the time scale set by the Brunt-Väisälä frequency. A new assumption is that the base state potential temperature is a slowly varying function of the vertical coordinate. It is this assumption that eliminates the energetic inconsistency discussed by Wilhelmson and Ogura (1972) for a non-isentropic base state. Another key result is that the dynamic pressure is an order of magnitude smaller than the first-order temperature and potential temperature. In agreement with observations, the kinetic energy is found to be an order of magnitude smaller than the first-order thermodynamic energy.

A set of six numerical simulations representing moderately deep moist convection is carried out. The base state is an idealized maritime tropical sounding with no vertical wind shear. The first calculation (Run A) shows the growth and dissipation of a typical shower cloud. The remaining calculations have small changes in either initial conditions or model equations from Run A. These calculations indicate the sensitivity of the present model to different approximations and give additional evidence for the validity of the scale analysis.

1. Introduction

In this study a scale analysis is carried out to examine the set of anelastic equations used to represent deep moist convection in the atmosphere. A key component of the present analysis is the assumption that the base state potential temperature $\theta_0(z)$ is a slowly varying function of the vertical coordinate z. Because of this assumption, the present study has its primary validity for deep convection confined to the troposphere. For severe mid-latitude convection, where the clouds make significant penetrations above the tropopause, the present analysis is expected to have limited validity.

There have been several earlier studies giving rigorous discussions of the deep anelastic equations (Ogura and Phillips, 1962; Dutton and Fichtl, 1969; Gough, 1969). These studies, however, leave unanswered several basic questions with respect to deep moist convection. In contrast to dry convection, it is desirable to have a non-isentropic base state in which $\theta_0(z)$ departs significantly from a constant value. Such a base state is expected to be relevant in deep moist convection due to the role of latent heat release. From a physical point of view, therefore, it is surprising to learn that the use of a non-isentropic base state leads to an energetic inconsistency (Wilhelmson and Ogura, 1972). This problem is resolved in the present scale analysis through the assumption that $\theta_0(z)$ is a slowly varying function of z.

Another relevant question is the role of the dynamic pressure in the calculation of the saturation vapor pressure e_s. In their scale analysis, Ogura and Phillips (1962) found an implicit relationship between the first-order potential temperature θ_1, the pressure function π_1, and the temperature T_1 for deep convection. Dutton and Fichtl (1969) obtain essentially the same result. Wilhelmson and Ogura (1972) have carried out numerical simulations comparing results with and without the inclusion of π_1 in the calculation of e_s. They find that the dynamically induced π_1 is an order of magnitude smaller than expected from the analysis of Ogura and Phillips and thus can be neglected in the calculation of e_s. These authors state that the smallness of π_1 is partly because the pressure diagnostic equation acts to smooth out the pressure distribution. In the present study the smallness of π_1 is a predicted result of the scale analysis.

The final question addressed by this scale analysis is the role of the environmental moisture field in the calculation of the base state pressure and potential temperature fields. To the authors' knowledge, all previous researchers have neglected this effect. The present work confirms that this moisture effect is not large enough to be physically significant.

The scale analysis and resulting conclusions are presented in Sections 2-6. In Section 7 some three-dimensional numerical calculations of moderately deep moist convection are discussed. The first calculation (Run A) shows the growth and decay of a typical shower cloud when no vertical wind shear is present. The remaining calculations have small changes in either initial conditions or model equa-

tions from Run A. These calculations show the sensitivity of the present model to different approximations and also give additional evidence for the validity of the scale analysis. Section 8 contains a summary and discussion for the present study.

2. The basic equations and non-dimensionalization

In the present discussion the dynamics and thermodynamics are kept to a maximum simplicity so that the main conclusions of the scale analysis can be shown more clearly. Thus the effects of eddy viscosity and eddy diffusivity are omitted. Likewise, the thermodynamics is limited to that involving warm rain processes with the latent heat of vaporization L being constant. The value assigned to L corresponds to a temperature of 0°C. Other physical constants include c_p, R_d and R_v which are respectively the specific heat of dry air at constant pressure, the gas constant for dry air and the corresponding gas constant for water vapor.

As in Ogura and Phillips (1962), it is convenient to represent the atmospheric pressure p' through the Exner function π, i.e.,

$$\pi = (p'/P)^\kappa, \quad \kappa = R_d/c_p,\qquad(1)$$

where P is a reference pressure. Likewise, from the definition of potential temperature θ', we have the relation

$$T' = \pi\theta'.\qquad(2)$$

Throughout the present analysis primes indicate that the respective variables are dimensional. Dimensional constants, however, do not have primes.

a. The basic equations

The basic equations for continuity, momentum, thermodynamics, water vapor mixing ratio q_v, cloud water mixing ratio q_c and rain water mixing ratio q_r are given in dimensional form by

$$\frac{\partial\rho'}{\partial t'} + \nabla'\cdot\rho'\mathbf{V}' = 0,\qquad(3)$$

$$\frac{\partial\mathbf{V}'}{\partial t'} + (\mathbf{V}'\cdot\nabla')\mathbf{V}'$$
$$= -c_p\theta'(1 + 0.608q_v)\nabla'\pi - g\mathbf{k}(1 + q_c + q_r),\qquad(4)$$

$$c_p\pi\left[\frac{\partial\theta'}{\partial t'} + (\mathbf{V}'\cdot\nabla')\theta'\right] = L(C_d' - E'),\qquad(5)$$

$$\frac{\partial q_v}{\partial t'} + (\mathbf{V}'\cdot\nabla')q_v = -C_d' + E',\qquad(6)$$

$$\frac{\partial q_c}{\partial t'} + (\mathbf{V}'\cdot\nabla')q_c = C_d' - A',\qquad(7)$$

$$\frac{\partial q_r}{\partial t'} + (\mathbf{V}'\cdot\nabla')q_r - \frac{1}{\rho'}\frac{\partial}{\partial z'}(\rho'V_T'q_r) = -E' + A',\qquad(8)$$

where ρ' is the density of air, $\mathbf{V}'$ the vector velocity of the air, V_T' the fall velocity of rain water, C_d' the condensation (evaporation) of cloud water, E' the evaporation of rain water, A' the total conversion of q_c into q_r, g the acceleration of gravity and $\mathbf{k}$ is the unit vertical vector. The constant 0.608 in (4) is equal to $(R_v/R) - 1$. Note that π, q_v, q_c and q_r are not primed as they are nondimensional.

The liquid water heating term, which represents the exchange of heat between q_c and q_r and the air (Lipps and Hemler, 1980), has been neglected in the thermodynamic equation (5). A brief discussion of results from a more complete thermodynamic equation is given in Section 7 where numerical calculations are carried out. Also in Section 7 the total conversion A' of q_c into q_r is split into the two components A_a' and A_c' following the ideas of Kessler (1969). The form of A_a' and A_c' is given in Appendix A.

b. The non-dimensional variables

Since the scale analysis will be carried out using non-dimensional variables, the appropriate dimensional scaling parameters need to be determined. For this purpose the convective velocity W and length scale l, which are defined and discussed in Section 3, will be used. The reference pressure P in (1) is defined as the base state pressure at the surface ($z' = 0$) and the base state potential temperature at the surface is defined as θ_{00}. Thus an appropriate scaling for the density is $\rho_{00} = P/R_d\theta_{00}$.

The set of non-dimensional variables already includes π, q_v, q_c and q_r. Using the above scaling parameters the remaining variables can be put into the non-dimensional forms

$$\begin{aligned}
&\theta = \theta'/\theta_{00}, \quad T = T'/\theta_{00}, \quad p = p'/P, \quad \rho = \rho'/\rho_{00}\\[4pt]
&C_d = C_d'l/W, \quad E = E'l/W, \quad A = A'l/W, \quad V_T = V_T'/W\\[4pt]
&\mathbf{V} = \mathbf{V}'/W, \quad x = x'/l, \quad y = y'/l, \quad z = z'/l, \quad t = t'W/l
\end{aligned}\qquad(9)$$

As implied by these relations, Cartesian coordinates are used with x', y' and z' scaled by l and the time t' scales by l/W. Using (9) Eqs. (3)–(8) will be discussed in non-dimensional form in the remainder of the present analysis. It is noted that the non-dimensional form of (2) is simply $T = \pi\theta$. Also, the non-dimensional form of (2) is simply $T = \pi\theta$. Also, the non-

dimensional parameter

$$L_c = L/c_p\theta_{00}\qquad(10)$$

will multiply $(C_d - E)$ in the thermodynamic equa-

tion. For typical atmospheric conditions $L_c \approx 8.3$.

In the following scale analysis L_c will be treated as of order unity. Although $L_c \approx 8.3$ may seem large compared to unity, it is small compared to the inverse of the primary expansion parameter ϵ. As seen below $\epsilon^{-1} \sim 100$.

3. The scale analysis assumptions

a. The parameters ϵ and δ

The first assumption of the present study is the existence of the two small parameters ϵ and δ. The first of these is the most important and is defined by

$$\epsilon = \Delta\theta_c/\theta_{00}, \qquad (11)$$

where $\Delta\theta_c$ is a characteristic value of the (dimensional) potential temperature excess in the clouds. This parameter is a measure of the strength of the moist convection. The second parameter δ is a measure of the water vapor present in the cloud environment and is defined as the value of the base state mixing ratio q_v at $z = 0$. In this analysis it is assumed that ϵ and δ are the same order of magnitude:

$$\delta = D\epsilon, \quad D \sim 1. \qquad (12)$$

Typical values of δ and ϵ are the order of 10^{-2}.

All dependent variables are expanded as power series in ϵ and δ. The initial form of this expansion is given by

$$\rho = \rho_0(z) + \cdots$$

$$\mathbf{V} = \mathbf{V}_0(x, y, z, t) + \cdots$$

$$
\begin{aligned}
T &= T_0(z) &&+ \epsilon T_1 (x, y, z, t) + \cdots \\
\theta &= \theta_0 (z) + \delta\theta_\delta (z) &&+ \epsilon\theta_1 (x, y, z, t) + \cdots \\
\pi &= \pi_0(z) + \delta\pi_\delta (z) &&+ \epsilon\pi_1 (x, y, z, t) + \cdots \\
q_v &= \delta q_{v\delta}(z) &&+ \epsilon q_v (x, y, z, t) + \cdots \\
q_c &= &&\epsilon q_{c1} (x, y, z, t) + \cdots \\
q_r &= &&\epsilon q_{r1} (x, y, z, t) + \cdots \\
C_d &= &&\epsilon C_{d1}(x, y, z, t) + \cdots \\
E &= &&\epsilon E_1 (x, y, z, t) + \cdots \\
A &= &&\epsilon A_1 (x, y, z, t) + \cdots
\end{aligned}
\qquad (13)
$$

$$V_T = V_{T0}(x, y, z, t) + \cdots$$

where it is noted that $\mathbf{V}$ is the total vector velocity rather than the horizontal component as in Ogura and Phillips (1962). Higher order terms not important in the present analysis have been omitted above. The base state variables in (13) are ρ_0, T_0, θ_0, π_0, θ_δ, π_δ and $q_{v\delta}$. It is assumed that T_0 and $q_{v\delta}$ are observed. The remaining base state variables can be obtained from T_0 and $q_{v\delta}$ using hydrostatics. This procedure is outlined in Section 5. It should be noted that the base state density $\rho_0(z)$ can be obtained from T_0, π_0 and the equation of state. As in Ogura and Phillips (1962), higher order terms in ρ and $\mathbf{V}$ will not appear in the equations below.

The variables θ_δ and π_δ exist due to the finite water vapor mixing ratio $q_{v\delta}$ in the base state. The definition of δ requires $q_{v\delta}(0) = 1$. Since $T_0(z)$ is the observed base state temperature, there is no δ component in the temperature field.

After the primary results have been obtained below, it will be seen that a modified form of (13) is appropriate. The final form of the power series expansion is given by Eq. (40) in Section 5.

b. Other scale analysis assumptions

In addition to the assumption of the small parameters ϵ and δ, the present scale analysis has four primary assumptions.

1) The time scale τ is set by the inverse of the Brunt-Väisälä frequency N:

$$\tau \sim N^{-1}, \quad N^2 = \frac{g}{\theta_{00}} \frac{\Delta\theta_T}{d}, \qquad (14)$$

where $\Delta\theta_T$ is the change in the (dimensional) base state potential temperature through the depth d of the troposphere. As in Ogura and Phillips (1962), the above condition on τ and the existence of the small parameters ϵ and δ imply that acoustic waves are absent. The following set of equations is therefore anelastic. The continuity equation to leading order is given by

$$\nabla \cdot \rho_0\mathbf{V}_0 = 0. \qquad (15)$$

2) The first-order buoyancy and the vertical ac-

celeration are required to be the same order of magnitude in the vertical momentum equation. Since the first-order buoyancy $\sim g\epsilon$ and the vertical acceleration $\sim W^2/l$, this balance is expressed by

$$G = g\epsilon l/W^2 \sim 1. \tag{16}$$

Note that $G \sim 1$ excludes moist convection on the scales of meso-β and meso-α (Fujita, 1963; Orlanski, 1975) from the present analysis. For these larger horizontal scales, the motion is either hydrostatic or quasi-hydrostatic (Orlanski, 1981). In that case it is not appropriate to set buoyancy and momentum terms the same order of magnitude.

3) The base state potential temperature $\theta_0(z)$ is a slowly varying function of z. Specifically, we assume that the dimensional vertical advection term $w'd\theta_0'/dz'$ is the same order of magnitude as the total time derivative of disturbance potential temperature $d\theta_1'/dt'$. Since $w'd\theta_0'/dz' \sim W\Delta\theta_T/d$, $d\theta_1'/dt \sim W\Delta\theta_c/l$ and $\epsilon = \Delta\theta_c/\theta_{00}$, this assumption is expressed by the relation

$$\frac{\Delta\theta_T}{\theta_{00}}\frac{l}{d} = B\epsilon, \quad B \sim 1. \tag{17}$$

In Eq. (9) of Section 2b the assumption $\tau = l/W$ has been made for the scaling of the non-dimensional variables. Combining (16) and (17) we find

$$\tau = lW^{-1}(GB)^{1/2}N^{-1}, \tag{18}$$

so that assumptions 2) and 3) and the scaling in Eq. (9) are mutually consistent with assumption 1).

4) The final assumption sets the order of magnitude of the mean lapse rate $\Delta\theta_T/d$ in the troposphere:

$$\frac{H}{d}\frac{\Delta\theta_T}{\theta_{00}} = \alpha, \quad \alpha \sim 0.5, \tag{19}$$

where $H = c_p\theta_{00}/g$. The length scale H is thus the height of an isentropic atmosphere. Noting that an equivalent form of (19) is

$$\Delta\theta_T/d = \alpha g/c_p, \tag{20}$$

we see that (19) implies $\Delta\theta_T/d \sim 5K \text{ km}^{-1}$.

An important relation is obtained from dividing (17) by (19), i.e.,

$$l/H = B\epsilon/\alpha. \tag{21}$$

Hence the length scale l is the order of ϵ smaller than H. This is a key result of the present analysis. In this discussion the length scale l should not be thought of as the depth of the total cloud but rather as the length scale of a typical eddy. Considering a thermal, the horizontal and vertical length scales are the same order of magnitude and both can be represented by l. Using (21) it might be tempting to argue that the continuity equation (15) could be simplified to the form of zero velocity divergence ($\nabla \cdot \mathbf{V}_0 = 0$). For deep convection, however, the total cloud depth is a large fraction of the depth d of the troposphere. Since the density ρ_0 has a significant variation over this depth, the full form of the continuity equation (15) should be retained.

The parameters B and G are given explicit values so that (17) and (16) can be considered as defining equations for l and W. Since there is no rigorous method to specify B and G from the scale analysis, any values assigned to these parameters are admittedly arbitrary. One obvious choice is to set $B = G = 1$. This choice, however, gives values of l and W which appear unrealistically small. In this study we set

$$G = 1, \quad B = 4. \tag{22}$$

The condition $G = 1$ appears reasonable for convection which has similar length scales in the horizontal and vertical. The second condition $B = 4$ then allows values of l and W which are compatible with the numerical calculations in Section 7. For those calculations we have $\epsilon \approx 10^{-2}$, $\Delta\theta_T/d \approx 5 \text{ K km}^{-1}$ and $\theta_{00} \approx 300 \text{ K}$. Using these values and Eqs. (17), (16) and (22) we find $l \approx 2.4 \text{ km}$ and $W \approx 16 \text{ m s}^{-1}$.

4. Thermodynamic and water substance equations

a. Thermodynamic equation

The variables $\theta_Z(Z)$ and $T_Z(Z)$ are useful in the discussion of the thermodynamics and energetics. They are defined by

$$\theta_0 = 1 + \left(\frac{\Delta\theta_T}{\theta_{00}}\right)\theta_Z(Z), \tag{23}$$

$$T_0 + \frac{d}{H}Z = 1 + \left(\frac{\Delta\theta_T}{\theta_{00}}\right)T_Z(Z), \tag{24}$$

where $Z = z'/d$. Thus Z represents the dimensional vertical coordinate z' scaled on d rather than l. Note that the dimensional form of the left side of (24) is $c_pT_0' + gz'$ which is the sum of the sensible heat plus potential energy in the base state.

The thermodynamic equation to leading order is given by

$$\pi_0\left\{\frac{\partial\theta_1}{\partial t} + (\mathbf{V}_0 \cdot \nabla)\theta_1 + w_0\left[B\frac{d\theta_Z}{dZ} + D\frac{d\theta_\delta}{dz}\right]\right\}$$
$$= L_c(C_{d1} - E_1), \tag{25}$$

where a factor of ϵ has been cancelled from both sides of (25) and terms of higher order than first order in ϵ have been dropped. The form of the expression multiplying the vertical velocity w_0 has been obtained by using (23), (17) and (12). Since the variation of θ_0 over the depth d of the troposphere is $\Delta\theta_T/\theta_{00}$, it can be seen from (23) that the vertical gradient $d\theta_Z/dZ \sim 1$. In Section 5 it will be shown that the term $Dd\theta_\delta/dz$ is actually the order of ϵ. Thus including this information

$$\pi_0 \left[\frac{\partial \theta_1}{\partial t} + (\mathbf{V}_0 \cdot \nabla)\theta_1 + w_0 B \frac{d\theta_Z}{dZ} \right] = L_c (C_{d1} - E_1) \quad (26)$$

is the final form of the thermodynamic equation to first order in ϵ. It is noted that the $Bw_0 d\theta_Z/dZ$ term is the same order of magnitude as the $(\mathbf{V}_0 \cdot \nabla)\theta_1$ term due to the assumption, as expressed by Eq. (17), that θ_0 is a slowly varying function of z.

b. Water substance equations

Equations to first order in ϵ for the mixing ratios q_{v1}, q_{c1} and q_{r1} are given by

$$\frac{\partial q_{v1}}{\partial t} + (\mathbf{V}_0 \cdot \nabla)q_{v1} + Dw_0 \frac{dq_{v\delta}}{dz} = -(C_{d1} - E_1), \quad (27)$$

$$\frac{\partial q_{c1}}{\partial t} + (\mathbf{V}_0 \cdot \nabla)q_{c1} = C_{d1} - A_1, \quad (28)$$

$$\frac{\partial q_{r1}}{\partial t} + (\mathbf{V}_0 \cdot \nabla)q_{r1} - \frac{1}{\rho_0} \frac{\partial}{\partial z} (\rho_0 V_{T0} q_{r1})$$

$$= -E_1 + A_1. \quad (29)$$

The correspondence between the previous dimensional equations [(5)–(8)] and the present dimensionless equations [(25)–(29)] can be clearly seen.

5. Analysis of the momentum equation

The full momentum equation (4) is first written in dimensionless form without neglecting any higher order terms. Scaling the variables as given in (9) yields

$$\frac{\partial \mathbf{V}}{\partial t} + (\mathbf{V} \cdot \nabla)\mathbf{V} = -\frac{G}{\epsilon}\frac{H}{l} \theta (1 + 0.608 q_v)\nabla \pi$$

$$- \frac{G}{\epsilon} \mathbf{k}(1 + q_c + q_r). \quad (30)$$

a. Hydrostatic equations

The leading order buoyancy and pressure gradient terms in (30) are inversely proportional to ϵ. From the power series expansion (13) it is seen that these terms represent the zeroth order hydrostatic relation

$$\frac{d\pi_0}{dz} = -\frac{l}{H}\frac{1}{\theta_0}. \quad (31)$$

Another relation which can be obtained from the zeroth order form of (2) is simply $T_0 = \pi_0\theta_0$. Combining this relation with (31) gives

$$\frac{d \ln\pi_0}{dz} = -\frac{l}{H}\frac{1}{T_0}. \quad (32)$$

Since T_0 is observed, π_0 can be calculated from (32) using the boundary condition $\pi_0 = 1$ at $z = 0$. Then θ_0 can be obtained from $T_0 = \pi_0\theta_0$.

The variables π_δ and θ_δ can also be calculated from hydrostatics using the observed $q_{v\delta}$. Since the tem-

perature T has no δ component, the total relation $T = \pi\theta$ has the δ component

$$0 = \frac{\pi_\delta}{\pi_0} + \frac{\theta_\delta}{\theta_0}. \quad (33)$$

The δ component of the pressure gradient term in (30) gives the hydrostatic relation

$$0 = -\theta_0 \frac{d\pi_\delta}{dz} - \frac{d\pi_0}{dz}(\theta_\delta + 0.608\theta_0 q_{v\delta}). \quad (34)$$

Dividing (34) by π_0 and using the relations (31), (33) and $T_0 = \pi_0\theta_0$ yields

$$\frac{d}{dz}\left(\frac{\pi_\delta}{\pi_0}\right) = 0.608 \frac{l}{H}\frac{1}{T_0} q_{v\delta}. \quad (35)$$

Eq. (35) can be solved for π_δ using the boundary condition $\pi_\delta = 0$ at $z = 0$. The potential temperature θ_δ can then be obtained from (33). Thus, in summary, the base state variables θ_0, π_0, θ_δ and π_δ can be obtained from hydrostatics assuming that $T_0(z)$ and $q_{v\delta}(z)$ are observed.

A significant conclusion can be inferred from (21). Since l/H is the order of ϵ, it follows from (35) that π_δ and therefore θ_δ are the order of ϵ. Thus the terms $\delta\theta_\delta$ and $\delta\pi_\delta$ in the expansion (13) are the order of $D\epsilon^2$ so that these contributions to the base state are negligible. This argument has used the assumption that the length scale l is the correct order of magnitude to represent the depth of the moist layer as determined by $q_{v\delta}$. This assumption appears reasonable.

b. The zeroth order momentum equation

A further look at the full pressure gradient term in (30) is required to obtain the zeroth order momentum equation. Specifically we consider the term

$$-\frac{G}{\epsilon}\frac{H}{l} \theta_0\nabla\epsilon\pi_1 = -G\frac{H}{l}\theta_0\nabla\pi_1.$$

Since $H/l \approx \epsilon^{-1}$ it follows that we must set $\pi_1 = \epsilon\pi_2$ because the highest order momentum terms are zeroth order in ϵ. Thus π_1 is the order of ϵ smaller than T_1 and θ_1 so that the first order expansion of $T = \pi\theta$ gives

$$T_1 = \pi_0\theta_1. \quad (36)$$

Hence T_1 and θ_1 are linearly related.

It is now shown that θ_0 can be put inside the pressure gradient term. Using (23) and (17) we find

$$-\theta_0\nabla\pi_2 = -\nabla(\theta_0\pi_2) + \mathbf{k}B\epsilon\pi_2 \frac{d\theta_Z}{dZ}. \quad (37)$$

Thus the term involving $d\theta_Z/dZ$ is the order of ϵ smaller than the $-\nabla(\theta_0\pi_2)$ term. This result is a direct consequence of (17), the assumption that θ_0 is a slowly varying function of z.

At this point the zeroth order momentum equation

can be derived. Using the power series expansion (13), Eq. (21) for H/l and the above results we find

$$\frac{\partial V_0}{\partial t} + (V_0 \cdot \nabla)V_0$$

$$= -\nabla\phi + G\mathbf{k}\left(\frac{\theta_1}{\theta_0} + 0.608q_{v1} - q_{c1} - q_{r1}\right), \quad (38)$$

where

$$\phi = G\frac{\alpha}{B}\theta_0\pi_2 . \quad (39)$$

The first two buoyancy terms are obtained from the first-order expansion of the pressure gradient term in (30) using (31) to represent $d\pi_0/dz$.

A complete set of basic equations has now been

obtained from the scale analysis for deep moist convection. The six equations [(15), (38) and (26)–(29)] can be solved for the six variables V_0, ϕ, θ_1, q_{v1}, q_{c1} and q_{r1} subject to the appropriate initial and boundary conditions. As is necessary for the anelastic equations, the pressure function ϕ is obtained from the solution of a Poisson equation which is derived by multiplying (38) by ρ_0 and taking the divergence of the resulting equation. The time tendency term vanishes by virtue of continuity (15) for the continuous Poisson equation. For numerical models this is not exactly so and is discussed in detail by Williams (1969).

c. Modified expansion of dependent variables

A modified form of the power series expansion (13) is now given using the results of the analysis above. For the primary dependent variables we have

$$\left.\begin{aligned}
\rho &= \rho_0(z) + \cdots \\
V &= V_0(x, y, z, t) + \cdots \\
T &= T_0(z) && + \epsilon T_1(x, y, z, t) + \cdots \\
\theta &= \theta_0(z) && + \epsilon\theta_1(x, y, z, t) + \cdots \\
\pi &= \pi_0(z) && + \epsilon^2\pi_2(x, y, z, t) + \cdots \\
q_v &= && \epsilon[Dq_{vb}(z) + q_{v1}(x, y, z, t)] + \cdots \\
q_c &= && \epsilon q_{c1}(x, y, z, t) + \cdots \\
q_r &= && \epsilon q_{r1}(x, y, z, t) + \cdots
\end{aligned}\right\}, \quad (40)$$

where the relation $\delta = D\epsilon$ has been used to eliminate the explicit δ dependence in the expansion of q_v. Thus no explicit dependence on δ remains in (40). For the dependent variables not shown in (40) the expansion remains the same as in (13).

6. Energetics

a. Kinetic energy

To obtain the kinetic energy equation, (38) is multiplied by $\rho_0 V_0$ (vector dot product) and written in flux form using continuity (15), i.e.,

$$\frac{\partial}{\partial t}\left(\frac{1}{2}\rho_0 V_0^2\right) + \nabla \cdot [\rho_0 V_0(\tfrac{1}{2}V_0^2 + \phi)]$$

$$= G\rho_0 w_0\left(\frac{\theta_1}{\theta_0} + 0.608q_{v1} - q_{c1} - q_{r1}\right). \quad (41)$$

The above equation will be integrated over a finite three-dimensional volume. In this and subsequent integrations it is assumed that the flux terms vanish upon integration. This assumption implies that no net energy of any form is advected into or out of the

volume of integration. Upon integration (41) yields

$$\frac{\partial}{\partial t}\int_V \left(\frac{1}{2}\rho_0 V_0^2\right)dV$$

$$= G\int_V \rho_0 w_0\left(\frac{\theta_1}{\theta_0} + 0.608q_{v1} - q_{c1} - q_{r1}\right)dV. \quad (42)$$

Hence the term on the right represents the total source of kinetic energy.

b. Thermodynamic energy

As discussed in Section 4a the thermodynamic equation to leading order is given by (26). If the factor π_0 on the left side of (26) is put inside the derivative terms and the relation (36) for T_1 is used, a prognostic equation for the temperature T_1 is obtained:

$$\frac{\partial T_1}{\partial t} + (V_0 \cdot \nabla)T_1 + Bw_0\frac{dT_z}{dZ}$$

$$= -\frac{l}{H}w_0\frac{\theta_1}{\theta_0} + L_c(C_{d1} - E_1). \quad (43)$$

For the present scale analysis this equation is equivalent to (26). Using Eqs. (17) and (24) it can be shown that the left side of (43) represents the total time derivative of the sensible heat plus potential energy.

Multiplying by ρ_0 and writing the equation in flux form, Eq. (43) becomes

$$\frac{\partial}{\partial t}(\rho_0 T_1) + \nabla \cdot \left\{\rho_0 \mathbf{V}_0 \left[\epsilon^{-1}\left(T_0 + \frac{d}{H}Z\right) + T_1\right]\right\}$$

$$= -\frac{l}{H}\rho_0 w_0 \frac{\theta_1}{\theta_0} + \rho_0 L_c (C_{d1} - E_1). \quad (44)$$

The component of the flux term proportional to ϵ^{-1} represents the base state sensible heat plus potential energy. It is seen that for the anelastic system the potential energy corresponding to $(d/H)Z$ has no first-order component. Integrating (44) over the volume gives

$$\frac{\partial}{\partial t}\int_V \rho_0 T_1 dV$$

$$= \int_V \rho_0 \left[-\frac{l}{H}w_0 \frac{\theta_1}{\theta_0} + L_c(C_{d1} - E_1)\right]dV. \quad (45)$$

The first and second terms on the right side of (45) represent the conversion of sensible heat into kinetic energy and the conversion of latent heat into sensible heat.

Since the potential energy has no first-order component, the relevant total energy equation involves the volume integral of the sum of the sensible heat, latent heat and kinetic energy. The time rate of change of total energy is given by

$$\frac{\partial}{\partial t}\int_V \rho_0 \left[T_1 + L_c q_{v1} + \frac{1}{G}\frac{l}{H}\frac{1}{2}\mathbf{V}_0^2\right]dV$$

$$= \int_V \rho_0 \left[\frac{l}{H}w_0(0.608 q_{v1} - q_{c1} - q_{r1})\right]dV. \quad (46)$$

Thus, in the present formulation, total energy is not conserved for deep moist convection. The lack of conservation is not due to the thermodynamics but rather is due to the water vapor and liquid water buoyancy terms in the w_0-momentum equation. The energetic inconsistency discussed by Wilhelmson and Ogura (1972) for a non-isentropic base state is not seen in Eq. (46). Evidently this problem has been eliminated since, as shown by (37), θ_0 can be put inside the pressure gradient term and the corresponding $d\theta_Z/dZ$ term [which would give rise to an additional term in (46)] is negligible.

The relation (21) indicates that the kinetic energy term on the left side of (46) and the buoyancy terms on the right side of (46) are the order of ϵ smaller than the sensible heat and latent heat terms. This result can be understood when it is remembered that

kinetic energy is scaled by W^2 whereas first-order sensible heat is scaled by $c_p\Delta\theta_c$. The ratio $W^2/(c_p\Delta\theta_c)$ gives

$$\frac{W^2}{c_p\Delta\theta_c} = \frac{1}{G}\frac{l}{H}, \quad (47)$$

which is just the term multiplying the kinetic energy $\frac{1}{2}\rho_0\mathbf{V}_0^2$ in (46). Thus the present scale analysis confirms that the usual practice of neglecting the kinetic energy budget when discussing the energetics of deep moist convection is legitimate to leading order.

c. Special case of dry convection

Several insights can be obtained by considering the special case of a dry atmosphere with no latent heat release. Under these conditions $q_{v1} = q_{c1} = q_{r1} = 0$, so that (46) becomes

$$\frac{\partial}{\partial t}\int_V \rho_0 \left[T_1 + \frac{1}{G}\frac{l}{H}\frac{1}{2}\mathbf{V}_0^2\right]dV = 0. \quad (48)$$

Hence, in distinction to the moist convection case, the above equation indicates a conservation of volume-integrated sensible heat plus kinetic energy.

For deep dry convection it is appropriate that the base state be an isentropic atmosphere with $\theta_0(z) = 1$. Thus the present case is now the same as that discussed by Ogura and Phillips (1962) and it can be shown that (48) is equivalent to their energy conservation equation (31). For this purpose, it is necessary to separate the sensible heat T_1 into two forms of energy. Since $T_1 = \pi_0\theta_1$ we have

$$I_\theta = \theta_1, \quad P_\theta = (\pi_0 - 1)\theta_1, \quad T_1 = I_\theta + P_\theta, \quad (49)$$

where P_θ is a potential energy and I_θ has the characteristics of an internal energy.

In the present context the thermodynamic equation (26) reduces to

$$\frac{\partial\theta_1}{\partial t} + (\mathbf{V}_0 \cdot \nabla)\theta_1 = 0, \quad (50)$$

which states the conservation of θ_1 following a parcel. Putting (50) in flux form and integrating over the volume yields

$$\frac{\partial}{\partial t}\int_V \rho_0 I_\theta dV = 0, \quad (51)$$

so that I_θ is conserved for dry convection. When (50) is multiplied by $\rho_0(\pi_0 - 1)$, put in flux form and integrated over the volume we obtain

$$\frac{\partial}{\partial t}\int_V \rho_0 P_\theta dV = -\frac{l}{H}\int \rho_0 w_0 \theta_1 dV. \quad (52)$$

Since $\theta_0 = 1$, the term on the right is equal to the conversion of potential energy into kinetic energy.

The volume integral of kinetic energy plus P_θ potential energy is therefore conserved. For an isentropic atmosphere, the form of $\pi_0(z)$ can be calculated as given by Ogura and Phillips. With $\pi_0(z)$ known, P_θ can be obtained from (49), i.e.,

$$P_\theta = -\frac{l}{H} z\theta_1, \qquad (53)$$

using the present notation. Hence, multiplying (48) by GH/l, the conservation of kinetic plus potential energy can be written as

$$\frac{\partial}{\partial t} \int_V \rho_0(\tfrac{1}{2}\mathbf{V}_0^2 - Gz\theta_1)dV = 0. \qquad (54)$$

The I_θ energy component vanishes in this equation by virtue of (51). Thus (54) corresponds to Eq. (31) in Ogura and Phillips (1962).

The energetics for deep moist convection can also be formulated in terms of I_θ and P_θ instead of the sensible heat T_1. In that case, Eq. (51) would contain a heat source term involving $L_c(C_{d1} - E_1)$ on the right side of the equation. The conversion of sensible heat into kinetic energy would again be accomplished through the conversion of P_θ potential energy into kinetic energy. The energy I_θ has the characteristics of an internal energy in that it does not get converted into kinetic energy. In the numerical calculations to follow the more familiar sensible heat T_1 will be analyzed. Although of possible interest in other studies, the alternative energy forms I_θ and P_θ will not be discussed further in this investigation.

7. Numerical calculations

In this section we present some three-dimensional numerical calculations of moderately deep moist convection associated with an idealized maritime tropical sounding. These calculations will indicate the general validity of the scale analysis and will show the sensitivity of the present model to different approximations. In addition, results from a more accurate form of the thermodynamic equation will be discussed.

a. The numerical model

A brief description of the numerical model is presented here. A more detailed discussion of the bulk cloud physics, subgrid-scale mixing processes, boundary conditions and finite difference methods is given in Appendix A. The numerical values of various constants used in the model calculations are given in Appendix B. In this section and Appendix A all variables are dimensional; the primes are dropped. The basic equations are the dimensional counterparts of (15), (38) and (26)–(29). The finite difference forms of (38) and (26)–(29) are obtained after multiplying

these equations by the density $\rho_0(z)$ and writing the nonlinear advection terms in flux form.

The numerical procedure for the present model is parallel to that discussed by Lipps (1977) for shallow moist convection. The domain of integration is a horizontally square area with $L_x = L_y = 12$ km and is bounded by rigid vertical boundaries at $z = 0$ and $z = 10$ km. Horizontal periodicity is required on the lateral side walls of the domain. The grid spacing is $\Delta x = \Delta y = 375$ m in the horizontal and $\Delta z = 250$ m in the vertical. Thus the domain involves a total of $(32 \times 32 \times 40)$ grid points. The time step is either $\Delta t = 5$ s or $\Delta t = 10$ s depending on the strength of the convection.

b. Initial conditions

The base state mixing ratio $\langle q_v \rangle$, potential temperature θ_0 and relative humidity are shown as functions of height in Fig. 1. The angle brackets denote a horizontal average. For the present calculations, the environment is assumed to have no vertical wind shear. The dashed curve shown along with the $\theta_0(z)$ profile represents the potential temperature calculated from Eq. (26) using parcel theory for moist saturated ascent. The cloud base is assumed to have the same temperature as the environment and to be located at $z = 625$ m. The parcel calculations are carried out as described by Lipps and Hemler (1980). The difference between the two potential temperature curves is a measure of the convective instability of the present base state. The maximum difference between the curves is approximately 4.5 K at mid-levels.

To initiate the convection, an axisymmetric heat flux distribution is applied at $z = 0$. This is accomplished by specifying the first-order potential temperature θ_1 at the lowest θ level (see Appendix A). The form of θ_1 is represented by a Gaussian function with the maximum value located at the center of the numerical model:

$$\theta_1(x, y) = A \exp\{\tfrac{1}{2}\alpha[(x/\Delta x)^2 + (y/\Delta y)^2]\}, \qquad (55)$$

where $A = 2.0$ K, $\alpha = 0.08$ and x and y are specified by

$$-\tfrac{1}{2}L_x \leqslant x \leqslant \tfrac{1}{2}L_x, \quad -\tfrac{1}{2}L_y \leqslant y \leqslant \tfrac{1}{2}L_y, \qquad (56)$$

where, as indicated above, $L_x = L_y = 12$ km. With the given value of α, the magnitude of $\theta_1(x, y)$ decreases rapidly as the distance from $x = 0$, $y = 0$ increases. For example, with $|x| = \tfrac{1}{4}L_x$, $\theta_1(x, y) < 2$ $\times 10^{-1}$ and with $|x| = \tfrac{1}{2}L_x$, $\theta_1(x, y) < 10^{-4}$.

The lower layers in the atmosphere near $x = 0$, $y = 0$ warm up rapidly due to the subgrid-scale vertical diffusion of heat. At 15 min a shallow cloud has
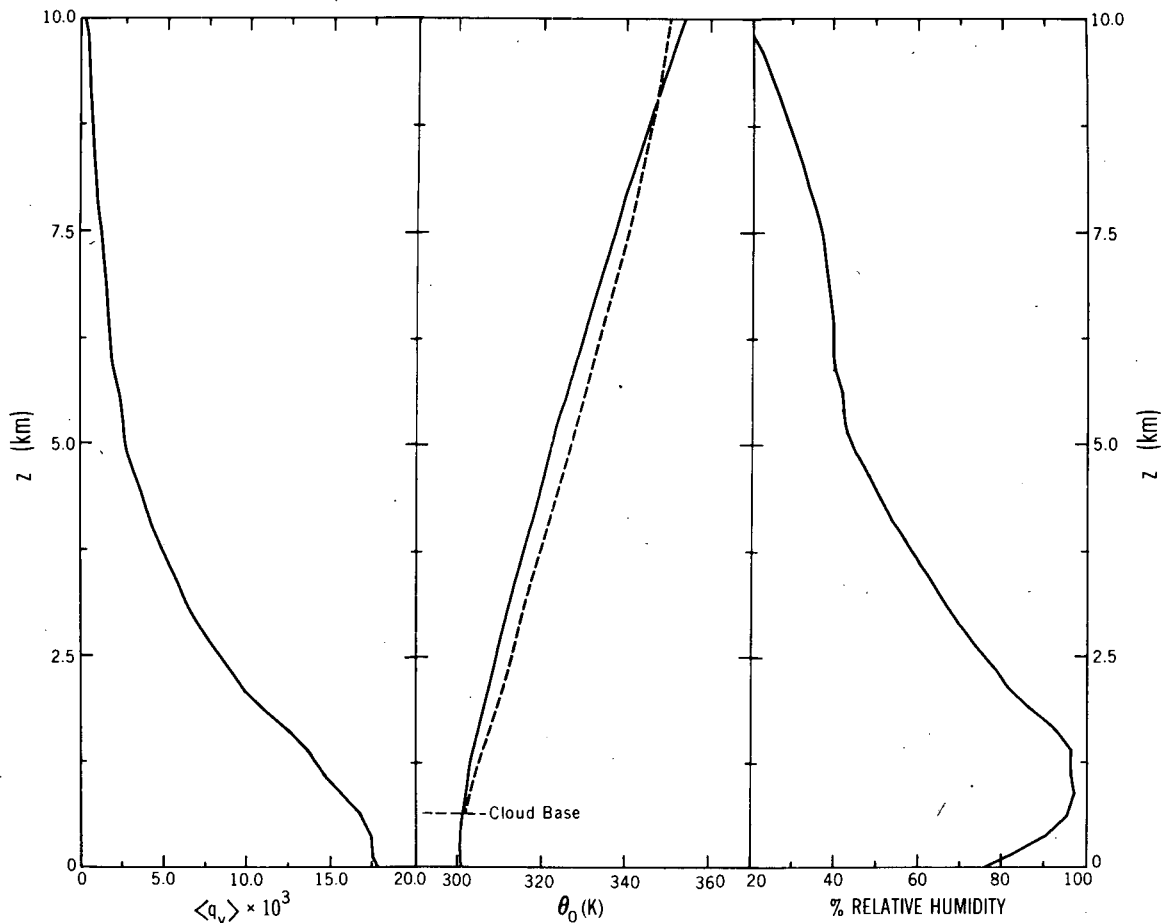
FIG. 1. Vertical sounding of the base state mixing ratio $\langle q_v \rangle$, potential temperature θ_0 and relative humidity. The angle braces indicate a horizontal average. See text for explanation of the dashed curve.

developed and $\theta_1(x, y)$ as given by (55) is turned off. For the remainder of the calculations the boundary condition of zero vertical heat flux is applied at $z = 0$.

c. Primary calculations

The primary calculations in the present study consist of a set of six runs. Run A is calculated with the above initial conditions and includes all of the approximations indicated to be valid by the scale analysis. The remaining five runs are calculations which represent small changes in either initial conditions or model equations from Run A. These changes are the same order of magnitude as terms neglected in the scale analysis. Run B is the same as Run A except that the base state mixing ratio $\langle q_v \rangle$ shown in Fig. 1 has been uniformly reduced by 1%. A comparison of Runs A and B will indicate in a quantitative way the sensitivity of the present model to changes in initial data.

Run C is the same as Run A except that the saturation vapor pressure e_s is included in the denominator of Eq. (A1) of Appendix A. This equation spec-

ifies the form of the saturation mixing ratio q_{vs} used in model calculations. In both Runs A and C the base state pressure $p(z)$ in (A1) is calculated neglecting the parameter δ in the scale analysis. Run D is the same as Run C except that first-order effects of the parameter δ are included. This change implies a slight modification of $p(z)$ from Run C and, more importantly, the dimensionless term $w_0 D d\theta_\delta/dz$ in Eq. (25) is now included in the thermodynamic equation.

In Run C_T the thermodynamic equation (26) is written in the form of (43) using the relation (36). Thus the thermodynamics is represented through a prognostic equation for the first-order temperature. For the present scale analysis Eqs. (26) and (43) should be identical and, for the compatible finite difference formulations, the numerical results are identical to within machine roundoff errors. In Run C_T the non-dimensional kinetic energy conversion term $-l/H(w_0\theta_1/\theta_0)$ in Eq. (43) has been neglected. In all other respects the calculations in Run C_T correspond to those in Run C.

In Run E the same approximations are used as discussed for Run D. The thermodynamics, however, is represented through Eq. (8) of Lipps and Hemler
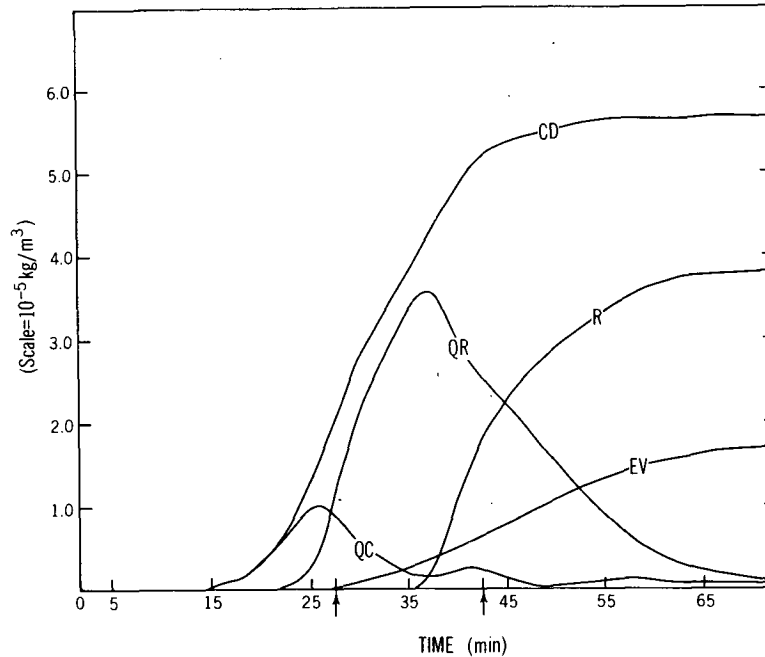
FIG. 2. The time history of Run A. For definitions of $R(t)$ and the volume-averaged variables $CD(t)$, $EV(t)$, $QR(t)$ and $QC(t)$ see Eq. (57) in the text. The two arrows along the t axis indicate the times of the flow fields plotted in Figs. 3 and 4.

(1980). In this equation the latent heat of vaporization L is a function of the base state temperature T_0 and the liquid water heating term is included. Although this equation is a more accurate representation of the thermodynamics, an order of magnitude analysis indicates that the change in thermodynamics from Run D to Run E is relatively small, involving terms the order of ϵ. For all of the calculations, viscous and diffusive effects are computed as described in Appendix A.

d. Discussion of Run A

In Run A the numerical calculations indicate the development and decay of a convective shower cloud similar to that discussed by Byers and Braham (1949) for the case of weak or no vertical wind shear. The total simulation was carried out for 72.5 min of real time.

TABLE 1. Maximum values of vertical velocity w, disturbance potential temperature θ'_1, cloud top Z_T, rainfall TR, kinetic energy PK, and sensible heat SH for the six numerical calculations.

Run	w (m s^{-1})	θ'_1 (K)	Z_T (m)	TR (cm)	$PK \times 10^{-3}$ (J m)	$SH \times 10^{-5}$ (J m)
A	21.9	3.40	7375	4.30	2.73	11.79
B	20.8	3.13	7125	3.99	2.19	10.53
C	18.9	3.03	7125	3.54	1.67	9.11
C_T	19.3	3.08	7125	3.58	1.72	9.43
D	20.4	3.22	7375	3.80	2.00	10.39
E	19.4	3.04	7125	3.55	1.85	9.35

1) TIME HISTORY OF RUN A

The time history of Run A is shown in Fig. 2 where the horizontally averaged rain $R(t)$ at the ground is compared with the volume-averaged variables $CD(t)$, $EV(t)$, $QR(t)$ and $QC(t)$ associated with the bulk cloud physics. These variables are defined by

$$
\left.
\begin{aligned}
R(t) &= d^{-1} \int_0^t \langle \rho_0 V_T q_r \rangle dt' \\
CD(t) &= \int_0^t \{\rho_0 C_d\} dt' \\
EV(t) &= \int_0^t \{\rho_0 E\} dt' \\
QR(t) &= \{\rho_0 q_r\} \\
QC(t) &= \{\rho_0 q_c\}
\end{aligned}
\right\} , \quad (57)
$$

where the braces represent a volume average. From the above definitions it is seen that continuity of water content implies

$$ CD = R + EV + QR + QC. \qquad (58) $$

The curves plotted in Fig. 2 appear typical of a convective shower cloud with no vertical wind shear present. The convection initially develops slowly so that by 15 min a small amount of cloud water QC is present. By 25 min QC is near its maximum and a strong conversion of QC into QR is starting to occur. At 36 min QR is near its maximum and heavy

rainfall has just begun at the ground. Most of the rain at the ground falls within the next 18 min. By the end of the run ($t = 72.5$ min) the cloud is well into the dissipation stage.

In order to give physical significance to the magnitudes of QC and QR, it is assumed that the active cloud is contained within a fraction α of the total volume. As will be seen below, Figs. 3 and 4 suggest that the estimate $\alpha = 10^{-2}$ is qualitatively correct. When expressed in terms of this fractional volume, the maximum cloud water $\alpha^{-1}QC \approx 1.0$ g m^{-3} at 25 min and the maximum rain water $\alpha^{-1}QR \approx 3.5$ g m^{-3} at 37 min.

The time history in Fig. 2 can be compared with that shown in Fig. 2 of Murray and Koenig (1972). Their calculations were carried out using a shallow axisymmetric model with the grid intervals $\Delta r = \Delta z = 200$ m. The basic sounding (San Juan, P.R., 2300 GMT 20 August 1963) and the initial disturbance were the same as used by Murray (1970). For Run 2 of their calculations the maximum vertical velocity was 13.9 m s^{-1} and the average rainfall (over a disk 300 m in radius) was 0.64 cm. The corresponding values for Run A are $w_{max} = 21.9$ m^{-1} s and the average rainfall (over a disk 562.5 m in radius) of ~3.10 cm. The maximum cloud top (determined by q_c) appeared to be about 4.0 km in their study whereas in Run A the cloud top reached 7.375 km (see Table 1).

In spite of the more intense convection in Run A, a comparison of Run A with Murray and Koenig's Run 2 shows that the time histories have much in common. The time required for the formation of cloud water QC and rain water QR and for the fallout of rain R are very similar. In Run A the time required for the rain to reach the ground is somewhat longer. This delay is associated with the greater heights to which the rain water is advected before falling out (see Figs. 3c and 4c). Also note that QC has secondary maxima at 41 and 56 min in Run A whereas the shallow convection run has only the primary maximum in QC at 25 min.

2) VERTICAL CROSS SECTIONS FOR RUN A

Flow patterns in Run A are shown for the times $t = 27.5$ min and 42.5 min in Figs. 3 and 4. These times are noted by the two arrows along the t axis in Fig. 2. Fig. 3 is plotted at the time of maximum vertical velocity and 2.5 min past the time of maximum θ'_1 in the simulation. Vertical sections of the vector wind field, the disturbance θ'_1 and q'_v fields, and the q_c and q_r fields are shown in Figs. 3a–3c. The shaded area represents the cloud. These sections are limited to the central half of the total x–z cross section. The disturbance potential temperature θ'_1 and disturbance mixing ratio q'_v are defined as deviations from the horizontal average $\langle\theta_1\rangle$ and $\langle q_v\rangle$, respectively.

The vector velocity field in Fig. 3a indicates a strong positive w through the depth of the cloud, with the maximum $w = 21.9$ m s^{-1} on the cloud axis at the height $z = 4.75$ km. A strong horizontal gradient in w exists at the cloud side boundaries with negative w outside the cloud. The largest negative $w = -3.6$ m s^{-1} and is located just outside the cloud at the height $z = 3.75$ km. The data in Fig. 3b indicate a warm moist cloud with strong evaporative cooling at the cloud top and sides. Evaporative cooling and upward motion near cloud base is apparently giving rise to the cool moist tongue of air oriented at approximately a 45° angle from cloud base. As seen in Fig. 3c, cloud water q_c is being converted into rain water q_r in the upper levels of the cloud where the vertical velocity and the condensation are the largest. At this stage in the cloud's development, the vertical velocity is strong enough to hold the rain water q_r in the upper part of the cloud.

The same flow fields are plotted in Fig. 4 at $t = 42.5$ min of Run A. At this time the cloud top has just reached its maximum height and heavy rain is falling at the ground. The cloud circulation has decreased sharply in intensity with a maximum $w = 9.0$ m s^{-1} located at $z = 6.50$ km. As seen in Fig. 4a, the circulation in the upper part of the cloud appears to closely approximate a vortex ring with rising motion inside the cloud and sinking motion just outside the cloud. This aspect of the cloud circulation and the circulation shown in Fig. 3a appear to follow the descriptive discussion given by Murray and Koenig (1972). Another feature which is prominent in Fig. 4a is the relatively large area of downward motion above the cloud top. This downward motion appears responsible for the positive θ'_1 and negative q'_v above the cloud as shown in Fig. 4b.

Strong evaporative cooling[1] is again indicated at the cloud top and sides by the negative values of θ'_1. The maximum $\theta'_1 \approx 1.6$ K at $z = 3.50$ km is in the lower portion of the cloud where $w \approx 5$ m s^{-1} and the cloud width is less. Another area with $\theta'_1 > 1.0$ K is seen below cloud base in the region of the strong downdraft. Here the adiabatic warming due to downward motion more than compensates for the evaporative cooling in this relatively moist air. This warming effect has been seen in earlier numerical simulations as well. It is shown very strongly in Fig. 6 of Miller and Pearce (1974) and to a much lesser degree in the axisymmetric model results of Soong and Ogura (1973).

The fallout of precipitation below cloud base seen in Fig. 4c is associated with a maximum downdraft of $w = -3.5$ m s^{-1} at $z = 0.5$ km. At lower levels

---

[1] This conclusion is confirmed by cloud water evaporation data which infer a maximum evaporative cooling rate of 1.9 K min^{-1} at cloud top.
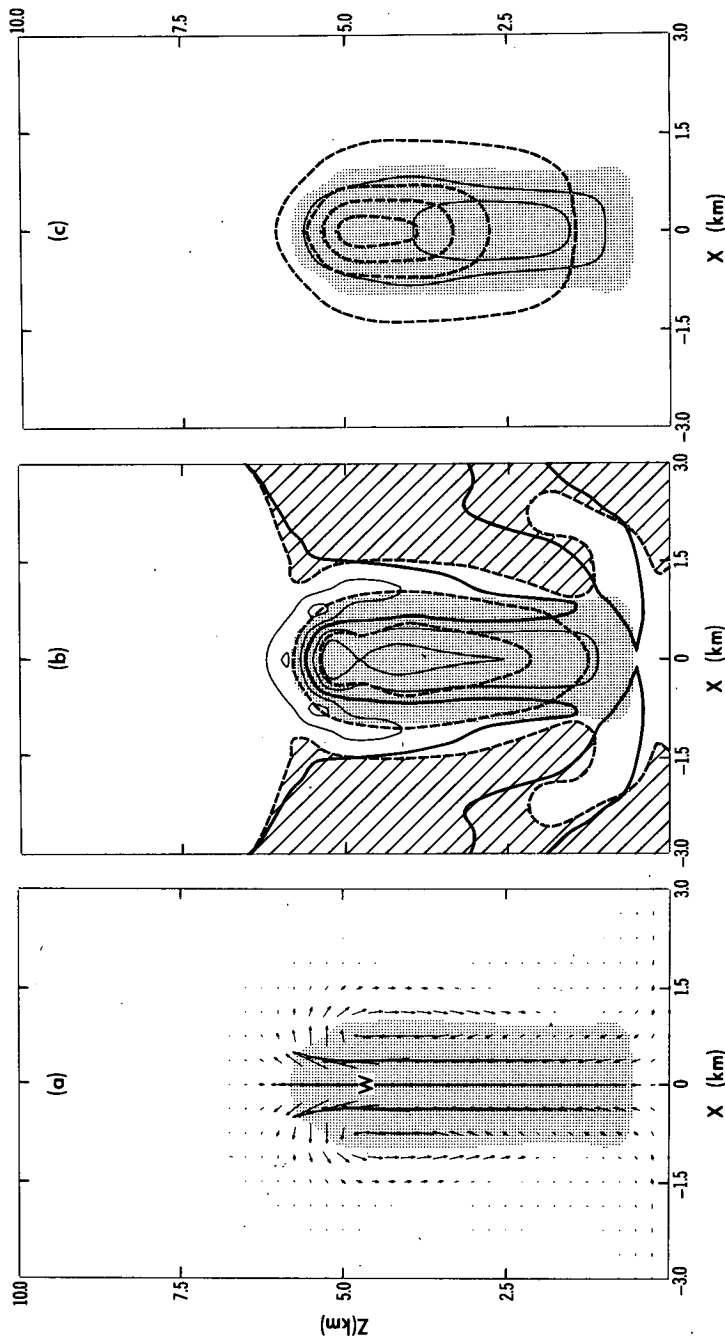
FIG. 3. Flow fields at $t = 27.5$ min of Run A. Shaded area represents the cloud. (a) Vector wind field. W indicates maximum vertical velocity (21.9 m s^{-1}). Length of arrows: 0.25 km = 4.0 m s^{-1}). (b) Disturbance θ'_1 (solid) and q'_v (dashed). The zero contour of θ'_1 is darker than other θ'_1 contours and areas of negative q'_v are hatched. Contour intervals for θ'_1 and q'_v are 1.0 K and 2.0 g kg^{-1}. (c) Contours of q_c (solid) and q_r (dashed). Contour intervals for q_c and q_r are 1.0 and 2.0 g kg^{-1}, respectively. Zero line for q_r is replaced by the 0.1 g kg^{-1} contour.
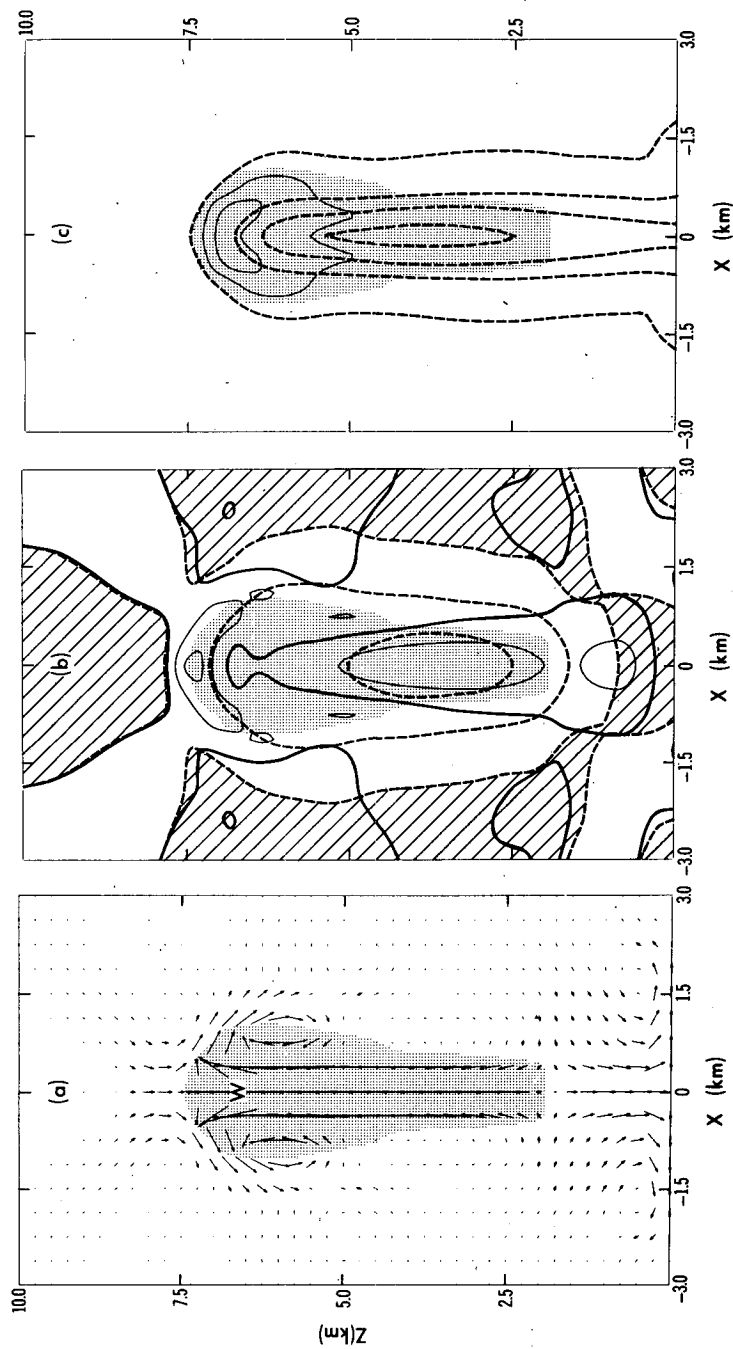
FIG. 4. As in Fig. 3 except at $t = 42.5$ min of Run A. W is 9.0 m s^{-1}. Length of arrows: 0.25 km = 2.0 m s^{-1}. Contour intervals for q_c and q_r are 0.5 and 2.0 g kg^{-1}.
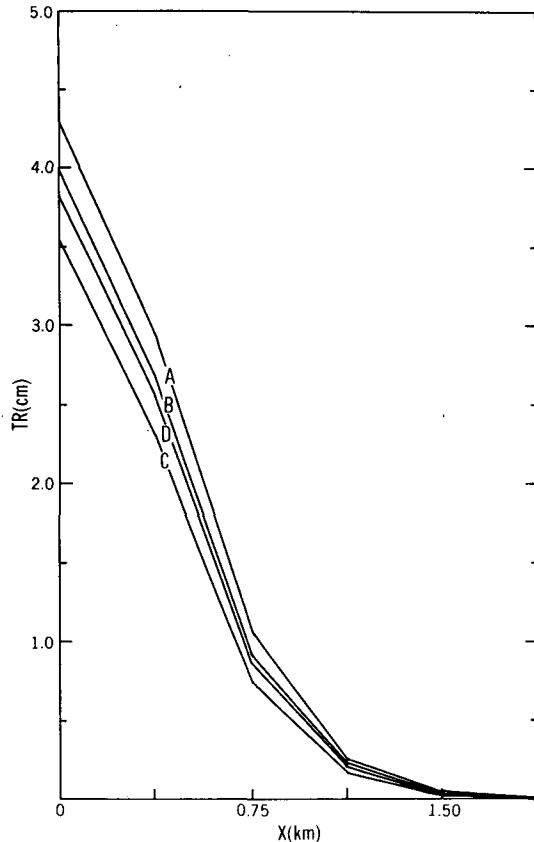
FIG. 5. Total accumulated rainfall TR as a function of x at t = 72.5 min. The cloud center is at x = 0. The four curves correspond to Runs A, B, C and D.

evaporative cooling dominates adiabatic warming so that the air is cool and dry near the surface. Thus at the surface $\theta'_1 \approx -0.7$ K and at z = 0.5 km the maximum drying effect is $q'_v \approx -0.5$ g kg^{-1}. Note that the cold air outflow is associated with a vortex circulation on either side of the cloud. These vortices remain weak and no secondary shower clouds develop.

In Figs. 3b and 4b a double maximum is seen in θ'_1 along the vertical cloud axis inside the cloud. Although multiple maxima in θ'_1 can occur in observed clouds, the authors believe the present double maxima are non-physical. The evaporative cooling gives rise to a very strong gradient in θ'_1 at the cloud top. Furthermore, the wavelength between the minimum θ'_1 associated with evaporative cooling and the relative minimum inside the cloud is $4\Delta z$. These considerations apply to both Figs. 3b and 4b. Another artificial effect is seen in Fig. 3c where rain water q_r diffuses above the cloud top and through the cloud sides without evaporating. This effect is minimized in Fig. 4c due to the lower relative humidity in the environment and the strong downward motion above the cloud. In spite of these deficiencies, the numerical simula-

tion of Run A has given reasonable results which will be compared with Runs B–E.

e. Comparison of Run A with other calculations

The total accumulated precipitation at t = 72.5 min is shown as a function of x in Fig. 5 for Runs A, B, C and D. The maximum precipitation is at the cloud center with the amount of rainfall decreasing rapidly with distance. At $2\Delta x$ (750 m) from the center the precipitation has been reduced to approximately one-fourth of its maximum value. The curves for Run C_T and Run E are not shown as they are very similar to the Run C curve. As may have been expected, the precipitation amount is sensitive to small changes in the model. In Run B the precipitation at cloud center is 7.2% less than in Run A and this reduction appears to be valid away from the cloud center as well. This decrease in rainfall is a direct consequence of the 1.0% reduction of the base state mixing ratio $\langle q_v \rangle$ used as initial data in Run B.

The reduction of rainfall at cloud center is 17.7% in Run C compared with Run A. This rather large decrease is directly attributable to the inclusion of e_s in the denominator of Eq. (A1). With this term included in (A1) the saturation mixing ratio q_{vs} is increased, thus delaying and reducing the amount of condensation C_d. This effect is accentuated in the present simulation because the cloud base is low and warm, typical of tropical maritime conditions. At cloud base the ratio $e_s/p(z) \approx 2.8 \times 10^{-2}$ which implies that q_{vs} is increased by 2.8% compared with the corresponding value in Run A. Thus the decrease in rainfall in Run C is seen to be compatible with the decrease in Run B.

The final curve in Fig. 5 indicates that the rainfall associated with Run D is larger than for Run C. This increase is a result of the inclusion of the first-order terms in δ in Run D. Specifically, the dimensional potential temperature gradient $d\theta_s/dz \approx -0.1$ K km^{-1} for vertical levels at and below cloud base ($z \leqslant 625$ m). This destabilizing effect included in the thermodynamic equation acts to increase the intensity of the convection in Run D.

Another comparison of the numerical data is shown in Table 1 where the maximum values of different variables are tabulated for each of the six runs. The rainfall TR is evaluated at the cloud center and the two forms of energy are represented by the vertical integrals

$$PK = \tfrac{1}{2} \int_0^d \rho_0 < \mathbf{V}^2 > dz$$
$$SH = c_p \int_0^d \rho_0 \pi_0 \langle \theta_1 \rangle dz \quad \left.\right\} . \qquad (59)$$

where $\langle \theta_1 \rangle$ = 0 at t = 0. Thus PK and SH are both equal to zero at the beginning of each run.

The data in Table 1 indicate that other parameters vary as much as the rainfall TR. The only exception is the cloud top height Z_T. For Runs A and D the cloud top is one grid interval higher than for the other runs. As seen by the comparison between Runs A and B, the model is sensitive to changes in initial conditions. This sensitivity, however, is not as strong as for the shallow convection study of Lipps (1977). The differences between Runs A, C and D parallel those shown in Fig. 5 and occur for the same reasons as discussed above.

A very close agreement is seen in Table 1 between Run C and Run C_T. Evidently the non-dimensional kinetic energy conversion term $-l/H(w_0\theta_1/\theta_0)$ neglected in Run C_T is not important for the present calculations. This conclusion is compatible with the scale analysis which indicates that $l/H \sim \epsilon$ from (21). Thus the kinetic energy conversion term is an order of ϵ smaller than the other terms in the thermodynamic equation (43).

The numerical calculations support the validity of the scale analysis in other ways as well. The values of θ_1' in Table 1 suggest a value $\epsilon \approx 10^{-2}$ as discussed in Section 3b. The data in this table also indicate a ratio $PK/SH \approx 0.25 \times 10^{-2}$ which is in agreement with $PK/SH \sim \epsilon$ as obtained in Section 6b. In Run A the maximum dynamic pressure $p_1 \approx 0.4$ mb which was observed at 25 min in the upper levels of the cloud circulation. This value of p_1 is small enough to consider the dynamic pressure a second-order effect as obtained in Section 5b. In some earlier calculations the pressure gradient term was written as $-c_p\theta_0\nabla\pi_1$ in one run and written as $-\nabla(c_p\theta_0\pi_1)$ in a second run. The rainfall TR differed by about 3% and maximum values of w, θ_1' and Z_T were virtually identical for the two runs. These calculations support the validity of Eq. (37), indicating that θ_0 can be put inside the pressure gradient term.

A comparison of Runs E and D shows the effect of a more accurate thermodynamic equation. As seen from Table 1, the values of the various parameters in Run E fall between those of Runs C and D, being on average closer to Run C. Thus, for the present calculations, the inclusion of the more accurate thermodynamics has an effect opposite in sign and slightly weaker in magnitude than that associated with the parameter δ. The apparent cancellation between these two effects is the reason for the very close agreement between Run C and Run E.

The relative behavior of Runs D and E can be examined in terms of the analysis of Lipps and Hemler (1980). The thermodynamic equations (5) and (25) in the present study correspond to the equation associated with the curves labeled "W" in Fig. 2 of that study. Likewise Run E corresponds to the axis of comparison in that figure. It was noted that the W curves were quite accurate for temperatures $\geqslant -10°C$. Since the presently simulated cloud temperatures are

warmer than $-10°C$ except near the cloud top, it could be anticipated that Runs D and E would have relatively good agreement. The form of the W curve in Fig. 2b of Lipps and Hemler also suggests that Run D would be slightly warmer than Run E at mid-levels in the cloud. The data for θ_1' in Table 1 indicate that this is indeed the case.

8. Summary and discussion

a. Scale analysis

In this study a scale analysis is carried out which is valid for deep moist convection in the troposphere. The primary new assumption of this analysis is that the base state potential temperature $\theta_0(z)$ is a slowly varying function of z. In Section 6b it is shown that this assumption eliminates the energetic inconsistency discussed by Wilhelmson and Ogura (1972). It should be noted that Dutton and Fichtl (1969) were able to obtain a consistent set of energy equations in their study. They defined a form of available potential energy which requires $\partial \ln\theta_0/\partial z = $ constant for energetic consistency. In the present study no such restriction is placed upon $\theta_0(z)$.

Another key result, as shown by Eq. (21), is that the convective length scale l is the order of ϵ smaller than the scale height H. Several important conclusions are associated with Eq. (21). The first is that the kinetic energy is the order of ϵ smaller than the first-order sensible heat. A second conclusion[2] is that the dynamic pressure π_1 is the order of ϵ smaller than T_1 and θ_1. Thus a linear relation [Eq. (36)] exists between T_1 and θ_1 so that there is no need of an implicit relationship, as thought necessary by Ogura and Phillips (1962), to calculate the saturation vapor pressure e_s when θ_1 is the prognostic variable. Hence the present analysis is in agreement with the numerical study of Wilhelmson and Ogura (1972). Another result due to π_1 being small is that the thermodynamics can be represented through a prognostic equation in T_1.

The importance of moisture in the base state is represented through the parameter δ in the scale analysis. The initial assumption of the present study is that δ and ϵ are both the same order of magnitude. By applying Eq. (21) to the hydrostatic equation (35), it is shown that the δ components of the base-state π and θ fields are the order of ϵ^2. Thus these contributions to the base state are predicted to be negligible.

---

[2] An important aspect of this conclusion was noted by a reviewer (Terry Clark). In Ogura and Phillips' (1962) scale analysis the base state was an isentropic atmosphere ($\theta_0 = $ constant). Clark (1979) points out that if the observed nonisentropic base state is used to obtain θ_0, T_0 and π_0, then π_1 is much smaller since a base state component $\pi_1(z)$ has been eliminated. In this case π_1 is equal to the perturbation π'' associated with the convection. Since Wilhelmson and Ogura (1972) and the present study both use observed nonisentropic base states, $\pi_1 = \pi''$ for both investigations. Thus both studies find $\pi'' \ll T_1$ or θ_1.

b. Numerical results

In Section 7 a set of six three-dimensional numerical calculations are discussed which represent moderately deep moist convection. The base state is an idealized maritime tropical sounding as shown in Fig. 1. The first calculation (Run A) has all of the approximations indicated to be valid by the scale analysis. The remaining runs have small changes in either initial conditions or model equations. A primary purpose of this set of calculations is to examine the validity of results obtained in the scale analysis.

The numerical simulation for Run A appears typical of a convective shower cloud with no vertical wind shear as discussed by Byers and Braham (1949). A couple of features shown in Fig. 4 at $t = 42.5$ min are considered noteworthy. One is the large area of downward motion above the cloud as seen in Fig. 4a. The second is the maximum in θ'_1 below cloud base as seen in Fig. 4b. Evidently, since mixing with the outside air is relatively weak, adiabatic warming dominates evaporative cooling in this moist region of the precipitation induced downdraft. Thus the authors view this maximum in θ'_1 as a physically realistic effect.

A comparison of Run A with the other calculations is shown in Fig. 5 and Table 1. Run B is the same as Run A except that the initial base state mixing ratio $\langle q_v \rangle$ has been uniformly decreased by 1%. The comparison of these two runs indicates the sensitivity of the present model to small changes in available moisture. The data in Table 1 indicate that the maximum values of w and θ'_1 and the total rainfall TR at cloud center decrease between 5 and 10% in Run B compared with Run A. This comparison suggests a limit to the accuracy to be expected from the present model. Since an uncertainty of 1% in initial data for $\langle q_v \rangle$ is not considered unreasonable, changes in model results no greater than 5–10% are not considered physically significant.

For Run C the maximum values of w and θ'_1 and the rainfall TR in Table 1 are decreased by $\sim 15\%$ from the corresponding values in Run A. As discussed in Section 7e, this reduction is due to the inclusion of e_s in the denominator of Eq. (A1) in Appendix A. This term increases the value of the saturation q_{vs} thus delaying and reducing the amount of condensation in Run C. Hence including this term has an effect approximately double of that in Run B where the initial $\langle q_v \rangle$ was reduced by 1%.

The non-dimensional term $-l/H(w_0\theta_1/\theta_0)$, representing the conversion of sensible heat into kinetic energy, has been omitted from the thermodynamic equation in Run C_T. In agreement with the scale analysis, the data in Table 1 indicate that this term is not important for the present calculations. As discussed in Section 7e, the numerical calculations support the validity of the scale analysis in several other ways as well.

The convection is slightly stronger in Run D than in Run C due to smaller values of the base state static stability below cloud base. As seen in Table 1, this δ-related effect results in the maximum values of w and θ'_1, and the rainfall TR being 5–8% larger in Run D than in Run C. Hence the change in the convection due to the inclusion of δ is not negligible; however, in view of the sensitivity of the model associated with Run B, this change cannot be considered physically significant.

In Run E the thermodynamics is represented by Eq. (8) of Lipps and Hemler (1980). As seen from Table 1, the inclusion of the more accurate thermodynamics has an effect opposite in sign and slightly weaker in magnitude than that associated with the parameter δ. The resulting very close agreement between Runs E and C is considered largely fortuitous. The important conclusion to be drawn from Run E is that the more accurate thermodynamics does not result in a large change in the convection for the present warm rain cloud model.

Calculations are currently being carried out using a numerical model analogous to Run C and a more realistic vertical sounding. The base state now represents a maritime tropical atmosphere from the surface to $z = 16$ km. Model simulations are being performed to determine the role of vertical wind shear and large-scale convergence in tropical moist convection.

APPENDIX A

Some Detailed Aspects of the Numerical Model

The numerical procedure parallels that of Lipps (1977) for shallow convection. Significant departures from that model (other than the straightforward modifications involving deep convection) are given in the discussion below.

1. The condensation C_d of cloud water q_c

Before calculating C_d, it is necessary to have explicit expressions for the saturation water vapor mixing ratio q_{vs} and the saturation vapor pressure e_s. The mixing ratio q_{vs} is given by

$$q_{vs} = \frac{0.622 e_s}{p(z) - e_s}, \tag{A1}$$

where $p(z)$ is the base state pressure. The variable $p(z)$ is discussed in more detail in Section 7.

The variation of L with temperature is taken into account in the calculation of e_s from the Clausius-Clapeyron equation. The form of L is given by

$$L = L_1 - L_2 T. \tag{A2}$$

Solving the Clausius-Clapeyron equation for $e_s(T)$ we find

$$e_s(T) = e_s(T_{00}) \exp\left[\frac{L_1}{R_v} \frac{(T_0 - T_{00})}{T_0 T_{00}} - \frac{L_2}{R_v} \ln \frac{T_0}{T_{00}}\right]$$

$$\times \exp\left[\frac{L\theta_1}{R_v T_0 \theta_0}\right], \tag{A3}$$

where T_{00} is a reference temperature, $T_0(z)$ the base state temperature, $\theta_0(z)$ the base state potential temperature and θ_1 the first-order potential temperature. T_{00} represents a temperature near cloud base. The approximation $\theta_1/\theta_0 \sim \epsilon$ has been used in the derivation of (A3).

When the air is saturated, the rate of condensation C_d is given by

$$C_d = \frac{\partial q_{va}}{\partial t} - \frac{\partial q_{vs}}{\partial t}, \tag{A4}$$

where $\partial q_{va}/\partial t$ represents the local increase in q_v if no condensation were present and $\partial q_{vs}/\partial t$ is the time rate of change of the saturated mixing ratio q_{vs}, i.e.,

$$\frac{\partial q_{va}}{\partial t} = -\frac{1}{\rho_0}\left[\frac{\partial}{\partial x_j}(\rho_0 u_j q_v) - \frac{\partial}{\partial x_j}(\overline{\rho_0 u_j' q_v'})\right], \tag{A5}$$

$$\frac{\partial q_{vs}}{\partial t} = \frac{L q_{vs}(1 + 1.608 q_{vs})}{R_v T_0 \theta_0} \frac{\partial \theta_1}{\partial t}, \tag{A6}$$

where the second term on the right in (A5) represents the subgrid-scale turbulent diffusion of q_v. Eq. (A6) is obtained by taking the time derivative of (A1) using (A3) to represent e_s. For calculations in which e_s is neglected in the denominator of (A1), the numerator in (A6) is reduced to $L q_{vs}$. In the majority of the numerical calculations, L is a constant in the thermodynamic equation. For these cases $L = $ constant in (A3) and (A6). For the one case in which L is not constant (see Section 7c), $L = L_1 - L_2 T_0$ in (A3) and (A6).

With the condensation C_d specified through (A4), (A5) and (A6), the prognostic equations for $\partial \theta_1/\partial t$ and $\partial q_v/\partial t$ are solved using a procedure analogous to that of Lipps (1977).

2. The bulk cloud physics

The bulk cloud physics parameterization follows the approach of Kessler, (1969). The total conversion A of cloud water q_c into rainwater q_r is split into two parts,

$$A = A_a + A_c, \tag{A7}$$

where A_a is the autoconversion and A_c the conversion due to accretion. In the present model A_a and A_c are given by

$$A_a = 10^{-3}(q_c - 1.5 \times 10^{-3} \rho_0^{-1}), \tag{A8}$$

$$A_c = 3.274 q_c q_r^{0.95}. \tag{A9}$$

In (A8) no autoconversion takes place for $\rho_0 q_c \leqslant 1.5$ g m^{-3}. In the model equations all units are MKS.

Expressions for the mean fall velocity V_T of the rain water q_r and for the evaporation E of rain water are required:

$$V_T = 5.32(\rho_0 q_r 10^3)^{0.2}, \tag{A10}$$

$$E = 0.0486(q_{vs} - q_v)(\rho_0 q_r)^{0.65}. \tag{A11}$$

In (A11) evaporation of rainwater occurs only in a subsaturated environment. The form of Eqs. (A8) and (A11) was originally proposed by Kessler (1969) whereas the form of Eqs. (A9) and (A10) was taken from the ideas of Liu and Orville (1969).

3. Subgrid-scale mixing and boundary conditions

a. Subgrid-scale mixing processes

The subgrid-scale turbulence parameterization is simplified from that presented in Lipps (1977). The terms involving thermal variance or total buoyancy variance have been dropped from the diagnostic equations of that study. The net effect is that the turbulence can be represented through an eddy viscosity K_m and an eddy diffusivity K_h. Following Deardorff (1972) we assume

$$K_h = 3 K_m. \tag{A12}$$

In discussing the subgrid-scale mixing, the dimensional forms of (38) and (26)–(29) are multiplied by ρ_0 and tensor notation is used. A frictional term of the form

$$F_i = \frac{\partial}{\partial x_j}\left[\rho_0 K_m\left(\frac{\partial u_i}{\partial x_j} + \frac{\partial u_j}{\partial x_i} - \frac{2}{3}\delta_{ij}\frac{\partial u_k}{\partial x_k}\right)\right] \tag{A13}$$

is added to the right side of Eq. (38). In Eqs. (26)–(29) the turbulent diffusion is represented through gradients of the subgrid-scale correlations $-\rho_0 \overline{u_j' \theta'}$, $-\rho_0 \overline{u_j' q_v'}$, $-\rho_0 \overline{u_j' q_c'}$ and $-\rho_0 \overline{u_j' q_r'}$. These correlations are given by

$$-\rho_0 \overline{u_j' \theta'} = \rho_0 K_h\left\{\frac{\partial}{\partial x_j}(\theta_0 + \theta_1)\right.$$

$$\left. + \frac{\delta_{j3} f \gamma}{1 + \beta\gamma}\left[\frac{\partial q_v}{\partial z} - \beta\frac{\partial}{\partial z}(\theta_0 + \theta_1)\right]\right\}, \tag{A14}$$

$$-\rho_0 \overline{u_j' q_v'} = \rho_0 K_h\left\{\frac{\partial q_v}{\partial x_j} - \frac{\delta_{j3} f}{1 + \beta\gamma}\right.$$

$$\left. \times \left[\frac{\partial q_v}{\partial z} - \beta\frac{\partial}{\partial z}(\theta_0 + \theta_1)\right]\right\}, \tag{A15}$$

$$-\rho_0 \overline{u'_j q'_c} = \rho_0 K_h \frac{\partial q_c}{\partial x_j}, \tag{A16}$$

$$-\rho_0 \overline{u'_j q'_r} = \rho_0 K_h \frac{\partial q_r}{\partial x_j}, \tag{A17}$$

$$\beta = \frac{L q_{vs}(1 + 1.608 q_{vs})}{R_v T_0 \theta_0}, \quad \gamma = \frac{L}{c_p \pi_0}, \tag{A18}$$

where f is the same parameter as used in Lipps (1977). Thus $f = 1$ inside of clouds, $f = 0$ outside of clouds, and $f = \frac{1}{2}$ on a cloud edge. Using (A1) and (A3) to represent q_{vs} and e_s, it was found that condensation effects identically vanish for the horizontal correlations ($j = 1, 2$) in (A14) and (A15). For consistency, in those calculations for which e_s is neglected in the denominator of (A1), the factor $(1 + 1.608 q_{vs})$ in (A18) is replaced by unity. In all calculations, $L = $ constant in (A18).

At this point it is appropriate to define the derivative notation

$$\frac{\partial \theta_e}{\partial x_j} \equiv \frac{\partial}{\partial x_j} (\theta_0 + \theta_1) + \gamma \frac{\partial q_v}{\partial x_j}, \tag{A19}$$

$$\frac{\partial \theta_v}{\partial x_j} \equiv \frac{\partial}{\partial x_j} (\theta_0 + \theta_1) + 0.608 \theta_0 \frac{\partial q_v}{\partial x_j}, \tag{A20}$$

where θ_e and θ_v are analogous to equivalent and virtual potential temperature. Defining the turbulent flux $\rho_0 \overline{u'_j \theta_e}$ and applying (A14) and (A15) yields

$$\rho_0 \overline{u'_j \theta_e} \equiv \rho_0 (\overline{u'_j \theta'} + \gamma \overline{u'_j q'_v}) = -\rho_0 K_h \frac{\partial \theta_e}{\partial x_j}. \tag{A21}$$

Thus (A14) and (A15) are compatible with the turbulent mixing of θ_e.

The remaining requirement of the present turbulence parameterization is to specify K_m and K_h. The eddy viscosity includes both deformation and unstable stratification effects (Lilly, 1962; Clark, 1979). The form of K_m is given by

$$K_m = c^2 \Delta^2 \left\{ \frac{D^2}{2} - \frac{2}{3} \left(\frac{\partial u_k}{\partial x_k} \right)^2 - 3\delta g \right.$$
$$\left. \times \left[(1 - f) \frac{1}{\theta_0} \frac{\partial \theta_v}{\partial z} + f \frac{\alpha}{\theta_0} \frac{\partial \theta_e}{\partial z} - \frac{\partial q_c}{\partial z} - \frac{\partial q_r}{\partial z} \right] \right\}^{1/2}, \tag{A22}$$

where $c = 0.21$, $\Delta = (\Delta x \cdot \Delta y \cdot \Delta z)^{1/3}$ and $\delta = 0, 1$; if the term in brackets is ≥ 0, $\delta = 0$; if this term is < 0, $\delta = 1$. The factor 3 multiplying δ represents the ratio K_h / K_m as specified by (A12). In addition we have defined

$$D^2 = \left(\frac{\partial u_i}{\partial x_j} + \frac{\partial u_j}{\partial x_i} \right) \left(\frac{\partial u_i}{\partial x_j} + \frac{\partial u_j}{\partial x_i} \right), \tag{A23}$$

$$\alpha(z) = \frac{1 + 0.608 \beta \theta_0}{1 + \beta \gamma}.$$

Note that $\alpha(z)$ is the same parameter as given by Eq. (47) of Lipps (1977). From (A12) K_h is specified by $K_h = 3K_m$.

b. Boundary conditions

Periodicity is required at the lateral side boundaries as indicated in Section 7. When discussing the upper and lower boundary conditions, it is necessary to note that the numerical grid is staggered in space as in Lipps (1977). Thus the vertical velocity w is evaluated on the upper and lower boundaries and the nearest grid points for u, v, θ, q_v, q_c and q_r are a one-half grid interval (125 m) from these boundaries. At the upper boundary, $w = 0$. At u, v, θ, q_v, q_c and q_r grid points 125 m below the top boundary, the vertical finite difference derivatives of $\rho_0 \overline{w'u'}$, $\rho_0 \overline{w'v'}$, $\rho_0 \overline{w'\theta'}$, $\rho_0 \overline{w'q'_v}$, $\rho_0 \overline{w'q'_c}$ and $\rho_0 \overline{w'q'_r}$ are required to vanish. These boundary conditions are the same as used by Klemp and Wilhelmson (1978).

At the lower boundary ($z = 0$), the vertical velocity $w = 0$ and the vertical derivatives of q_c and q_r are required to vanish. The values of u, v, θ and q_v are specified at their lowest vertical level which is located 125 m below the $z = 0$ surface. In the present calculations we set $u = v = 0$ and $q_v = $ constant at this level. At the beginning of the simulations, when surface heating is present, θ is required to vary as a Gaussian at its lowest level (see Section 7). Later, when the surface heating is turned off, the condition on θ is replaced by the condition $\rho_0 \overline{w'\theta'} = 0$ at $z = 0$.

The condition $q_v = $ constant at the lowest vertical level was intended to give a crude representation of the vertical moisture flux across an ocean surface. More recent calculations use a drag law formulation to represent surface boundary conditions.

4. Finite difference methods

The momentum equation and the θ and q_v equations are solved using centered time and space differences as in Lipps (1977). Instead of time smoothing every 30 time steps, a Robert (1966) time filter with $\epsilon = 0.4$ is used as in Clark (1979). In addition, small fourth-order horizontal damping terms have been added to these equations with $K_D \Delta t / (\Delta x)^4 = 0.0025$ as in Klemp and Wilhelmson (1978).

The prognostic equations for q_c and q_r are solved using the method given by Clark (1979). This method involves a hybrid finite difference scheme based on a second-order in space and first-order in time Crowley (1968) scheme and an upstream differencing scheme which is first-order in both space and time. The motivation for using this scheme is to eliminate the problem of numerically generated spurious negative values of q_c and q_r.

APPENDIX B

Numerical Values of Constant Coefficients

L constant latent heat of vaporization (0.2501×10^7 J kg^{-1})

c_p specific heat of dry air at constant pressure (1005.7 J kg^{-1} K^{-1})

R_d dry air gas constant (287.04 J kg^{-1} K^{-1})

R_v water vapor gas constant (461.50 J kg^{-1} K^{-1})

P reference pressure (1000 mb)

θ_{00} base state potential temperature at $z = 0$ (300.65 K)

d depth of troposphere in scale analysis; total depth in numerical model (10^4 m)

$\Delta\theta_T$ total change in base state potential temperature through depth d; in numerical model (52.85 K)

g acceleration due to gravity (9.781 m s^{-2})

T_{00} reference temperature (294.15 K)

$e_s(T_{00})$ saturated vapor pressure at temperature T_{00} (24.861 mb)

L_1 constant in Eq. (A2) for variable L (3.1447×10^6 J kg^{-1})

L_2 constant in Eq. (A2) for variable L (2357.2 J kg^{-1} K^{-1}).

REFERENCES

Byers, H. R., and R. R. Braham, 1949: *The Thunderstorm*. Govt. Printing Office, Washington, DC, 287 pp.

Clark, T. L., 1979: Numerical simulations with a three-dimensional cloud model: Lateral boundary condition experiments and multicellular severe storm simulations. *J. Atmos. Sci.*, **36**, 2191–2215.

Crowley, W. P., 1968: Numerical advection experiments. *Mon. Wea. Rev.*, **96**, 1–11.

Deardorff, J. W., 1972: Numerical investigation of neutral and unstable planetary boundary layers. *J. Atmos. Sci.*, **29**, 91–115.

Dutton, J. A., and G. H. Fichtl, 1969: Approximate equations of motion for gases and liquids. *J. Atmos. Sci.*, **26**, 241–254.

Fujita, T., 1963: Analytical mesometeorology: A review. *Severe Local Storms*, Meteor. Monogr., No. 27, Amer. Meteor. Soc., 77–125.

Gough, D. O., 1969: The anelastic approximation for thermal convection. *J. Atmos. Sci.*, **26**, 448–456.

Kessler, E., 1969: *On the Distribution and Continuity of Water Substance in Atmospheric Circulations*. Meteor. Monogr., No. 32, Amer. Meteor. Soc., 84 pp.

Klemp, J. B., and R. B. Wilhelmson, 1978: The simulation of three-dimensional convective storm dynamics. *J. Atmos. Sci.*, **35**, 1070–1096.

Lilly, D. K., 1962: On the numerical simulation of buoyant convection. *Tellus*, **14**, 148–172.

Lipps, F. B., 1977: A study of turbulence parameterization in a cloud model. *J. Atmos. Sci.*, **34**, 1751–1772.

——, and R. S. Hemler, 1980: Another look at the thermodynamic equation for deep convection. *Mon. Wea. Rev.*, **108**, 78–84.

Liu, J. Y., and H. D. Orville, 1969: Numerical modelling of precipitation and cloud shadow effects on mountain-induced cumuli. *J. Atmos. Sci.*, **26**, 1283–1298.

Miller, M. J., and R. P. Pearce, 1974: A three-dimensional primitive equation model of cumulonimbus convection. *Quart. J. Roy. Meteor. Soc.*, **100**, 133–154.

Murray, F. W., 1970: Numerical models of a tropical cumulus cloud with bilateral and axial symmetry. *Mon. Wea. Rev.*, **98**, 14–28.

——, and L. R. Koenig, 1972: Numerical experiments on the relation between microphysics and dynamics in cumulus convection. *Mon. Wea. Rev.*, **100**, 717–732.

Ogura, Y., and N. A. Phillips, 1962: Scale analysis of deep and shallow convection in the atmosphere. *J. Atmos. Sci.*, **19**, 173–179.

Orlanski, I., 1975: A rational subdivision of scales for atmospheric processes. *Bull. Amer. Meteor. Soc.*, **56**, 527–530.

——, 1981: The quasi-hydrostatic approximation. *J. Atmos. Sci.*, **38**, 572–582.

Robert, A. J., 1966: The integration of a low order spectral form of the primitive meteorological equations. *J. Meteor. Soc. Japan*, **44**, 237–245.

Soong, S.-T., and Y. Ogura, 1973: A comparison between axisymmetric and slab-symmetric cumulus cloud models. *J. Atmos. Sci.*, **30**, 879–893.

Wilhelmson, R., and Y. Ogura, 1972: The pressure perturbation and the numerical modeling of a cloud. *J. Atmos. Sci.*, **29**, 1295–1307.

Williams, G. P., 1969: Numerical integration of the three-dimensional Navier-Stokes equations for incompressible flow. *J. Fluid Mech.*, **37**, 727–750.